ORIGINAL PAPER

CrossMark

Estimating potential direct runoff for ungauged urban watersheds based on RST and GIS

Farid Radwan[1] · A. A. Alazba[1,2] · Amr Mossad[2,3]

Abstract

Estimating the potential direct runoff for urban watersheds is essential for flood risk mitigation and rainwater harvesting. Thus, this study aims to estimate the potential runoff depth based on the natural resources conservation service (NRCS) method and delineation of the watersheds in Riyadh, Saudi Arabia. To accomplish this objective, the geographic information systems (GIS) and remote sensing technique (RST) data were integrated to save time and improve analysis accuracy. The employed data include the digital elevation model (DEM), soil map, geology map, satellite images, and daily precipitation records. Accordingly, the hydrologic soil groups (HSG), the land use/land cover (LULC), and curve number (CN) were determined for each watershed in the study area. The results of this analysis show that the study area can be delineated into 40 watersheds with a total area of 8500 km^2. Furthermore, the dominant HSG is group D, which represents about 71% of the total area. The LULC maps indicate four major land types in the entire study area: urban, barren land, agricultural land, and roads. The CN of the study area ranges from 64 to 98, while the weighted CN is 92 for the city. The rainfall-runoff analysis shows that the area has a high and very high daily runoff (35–50 and > 50 mm, respectively). Therefore, in this case, the runoff leads to flooding, especially in the urban area and agricultural lands.

Keywords Rainfall-runoff · NRCS-CN · Urban watershed · HSG · LULC · RST & GIS

Introduction

Flash flooding is a rapid and extreme effect of rainfall in a very short period (Hoedjes et al. 2014; Starosolszky and Melder 2014; Archer and Fowler 2015; Deng et al. 2015). The enormous amounts of rainwater can be exploited for different applications such as rainwater harvesting, recharging artificial reservoirs, irrigation, and reuse to supply drinking water (Angelakis 2016; GhaffarianHoseini et al. 2016). However, such massive amounts of water are also catastrophic and can cause destruction (Abbas et al. 2016; Dale et al. 2016;

Karagiorgos et al. 2016). Rainfall water becomes a threat when flood control systems are unable to accommodate the enormous volumes of water during storms. Therefore, the massive amount of water may threaten regions, such as agricultural, industrial, and urban areas (Elfeki et al. 2017). Calculating the runoff volume is useful for mitigating flood risk and exploiting huge amounts of rainfall water (Masseroni et al. 2016). Many methods have recently been introduced to estimate the amount of runoff water, such as the peak discharge method, tabular method, unit hydrograph method, constant loss rate method, and initial loss-constant loss rate method (Moon et al. 2016; Nonglait and Tiwari 2016; Mistry et al. 2017). One widely used method to calculate runoff is the natural resources conservation service (NRCS) method, which was previously known as the soil conservation service (SCS) method (Pitt 1999; Patil et al. 2008; Ebrahimian et al. 2009; Bhagat 2016; Shah and Bhagat 2017). The NRCS method for estimating the runoff curve number (CN) was developed by the United States Department of Agriculture (USDA) (Cronshey 1986). This method depends on precipitation, potential maximum retention after runoff begins, and initial abstraction (Hong et al. 2007; Ebrahimian 2012; Ajmal et al.

✉ Farid Radwan
  fradwan@ksu.edu.sa

1   Alamoudi Water Research Chair, King Saud University, Riyadh, Saudi Arabia

2   Agricultural Engineering Department, King Saud University, Riyadh, Saudi Arabia

3   Agricultural Engineering Department, Ain Shams University, Cairo, Egypt

2016; Ryu et al. 2016; Abdullah et al. 2017; Singh et al. 2017). The potential maximum retention after runoff begins is related to the CN (Durán-Barroso et al. 2016; Lal et al. 2016). Hence, the NRCS method relies mainly on precipitation and the CN.

A particular CN for an area is associated with data of hydrologic soil group (HSG), land use/land cover (LULC), treatment, hydrologic condition, antecedent runoff condition (ARC), and integrated pervious and impervious areas (Mishra and Singh 2013; Ryu et al. 2016; Mahmoud and Gan 2018d). The HSG is very essential for categorizing different soils into specific groups according to their infiltration rates (NRCS 2007), which are similar in terms of physical and runoff characteristics. Factors affecting the HSG are saturated hydraulic conductivity of the layer of least transmissivity, depth to the water impermeable layer, and depth to the high water table. Of these, the most influential factor is hydraulic conductivity (Lee et al. 2016). According to NRCS, the HSG was initially classified into four groups, namely A, B, C, and D, and recently, three new dual groups of A/D, B/D, and C/D were added (NRCS 2009). In the four single groups, "A" refers to soils with high infiltration rates and low potential runoff; "D" represents soils with a low infiltration rate and high potential runoff; and "B" and "C" indicate moderate and slow infiltration rates, respectively (Shadeed and Almasri 2010; Ahmad et al. 2015).

The LULC data provides useful information for describing the land use and land cover types of a particular area. The extent of LULC covers several categories such as water bodies, agricultural land, built-up land, barren land, and roads (Fisher et al. 2005). The classification process of these categories is extensive and intensive work. Thus, the process of developing LULC datasets generally depends on satellite images (Mack et al. 2017; Zhang et al. 2017). The LULC developed through satellite images can distinguish land features into four classes, namely urban, barren land, agricultural land, and roads. Each of these has a unique CN value according to the infiltration rate. The CN value ranges from 0 to 100, which refers to low and high runoff extremes, respectively (Li et al. 2015). In general, land use change influencing local temperature and precipitation (Mahmoud and Gan 2018a; Mahmoud and Gan 2018b). The treatment describes the cultivation method used in agricultural lands including tillage, hoeing, sowing, contouring, and terracing (Cronshey 1986). Meanwhile, the hydrologic condition expresses runoff or infiltration under the treatment and cover type (Gajbhiye et al. 2014). The three cases of the hydrologic condition (good, fair, and poor) are given in descending order with respect to the infiltration rate (Cronshey 1986). Generally, a good hydrologic condition has high infiltration and low runoff. On the contrary, a poor hydrologic condition has low infiltration and high runoff. The ARC, or pre-storm soil moisture, is considered one important factor affecting the CN and is defined as the runoff potential index before the occurrence of storm events. There are three cases of ARC according to NRCS: I, II, and III (Cronshey 1986). The values of these cases are arranged in descending order with respect to soil moisture (Oliveira et al. 2016). Case (I) has dry soil but not to the wilting point, while in contrast, the case (III) has saturated soil as a result of heavy or light rainfall for the last 5 days. In general, the NRCS adopts the average case, II, to estimate CN values (Sartori et al. 2011), although the CN values should also be adjusted for the other two cases to avoid sudden jumps in runoff estimation. Furthermore, the CN value varies in the cases of connected or unconnected impervious areas. If the impervious areas are directly connected to the drainage system, water loss by infiltration does not occur (Cronshey 1986).

The potential runoff (Q) for every cell can be determined by the CN equation (Q = $\frac{(P-I_a)^2}{(P-I_a)+S}$) (Salih and Hamid 2017; Singh et al. 2017). From this equation, three factors influencing runoff are identified in units of millimeters (Anaba et al. 2017; Wang et al. 2017): (1) P—precipitation, (2) S—potential maximum retention after runoff begins, and (3) I_a—initial abstraction. Furthermore, an existent relationship is present between S (a function of CN) and I_a. The initial abstraction plays an essential role in prognosticating the potential runoff. According to NRCS (2007), the initial abstraction ratio (λ) is 0.2. Because this value is ambiguous, several researchers have conducted experiments in attempts to validate it. For example, some of these studies found that the ratio varies from 0.01 to 0.154, with an average value of 0.048 (Shi et al. 2009; Yuan et al. 2014). Thus, the more realistic ratio is 0.05 (Woodward et al. 2003; Beck et al. 2009; Ajmal and Kim 2014). A proper determination of CN and λ values is definitely reflected in obtaining the optimum potential maximum retention and then reflected in the estimation of potential direct runoff. Therefore, this study used the Sobhani formula (Sobhani 1976) to convert normal CN (CN_II) to the dry CN case (CN_I), moreover, the Hawkins formula (Hawkins et al. 1985) to convert normal CN (CN_II) to the wet CN case (CN_III).

Determining the Q through integrating geographic information systems (GIS) and remote sensing technique (RST) is a powerful technique that saves time and effort. As well as, the availability of precipitation data used in this technique which can be downloaded from the Climate Forecast System Reanalysis (CFSR) of the National Centers for Environmental Prediction (NCEP) (Dile and Srinivasan 2014; Fuka et al. 2014; Rajeevan 2017; Tirkey et al. 2017). Several studies have applied this integration to estimate potential runoff (Chavda et al. 2016; Harish et al. 2016; Jaber et al. 2016; Patel and Trivedi 2016). The GIS data in such studies have been used in watershed delineation, geo-referencing, digitizing, map projection, CN distribution, and runoff estimation. Meanwhile, RST has been utilized in classifying satellite images for LULC. Recently, the Riyadh metropolitan area, Saudi Arabia, experienced flash flooding that resulted in damages such as socioeconomic loss, soil erosion, land degradation, and vegetation loss in addition to
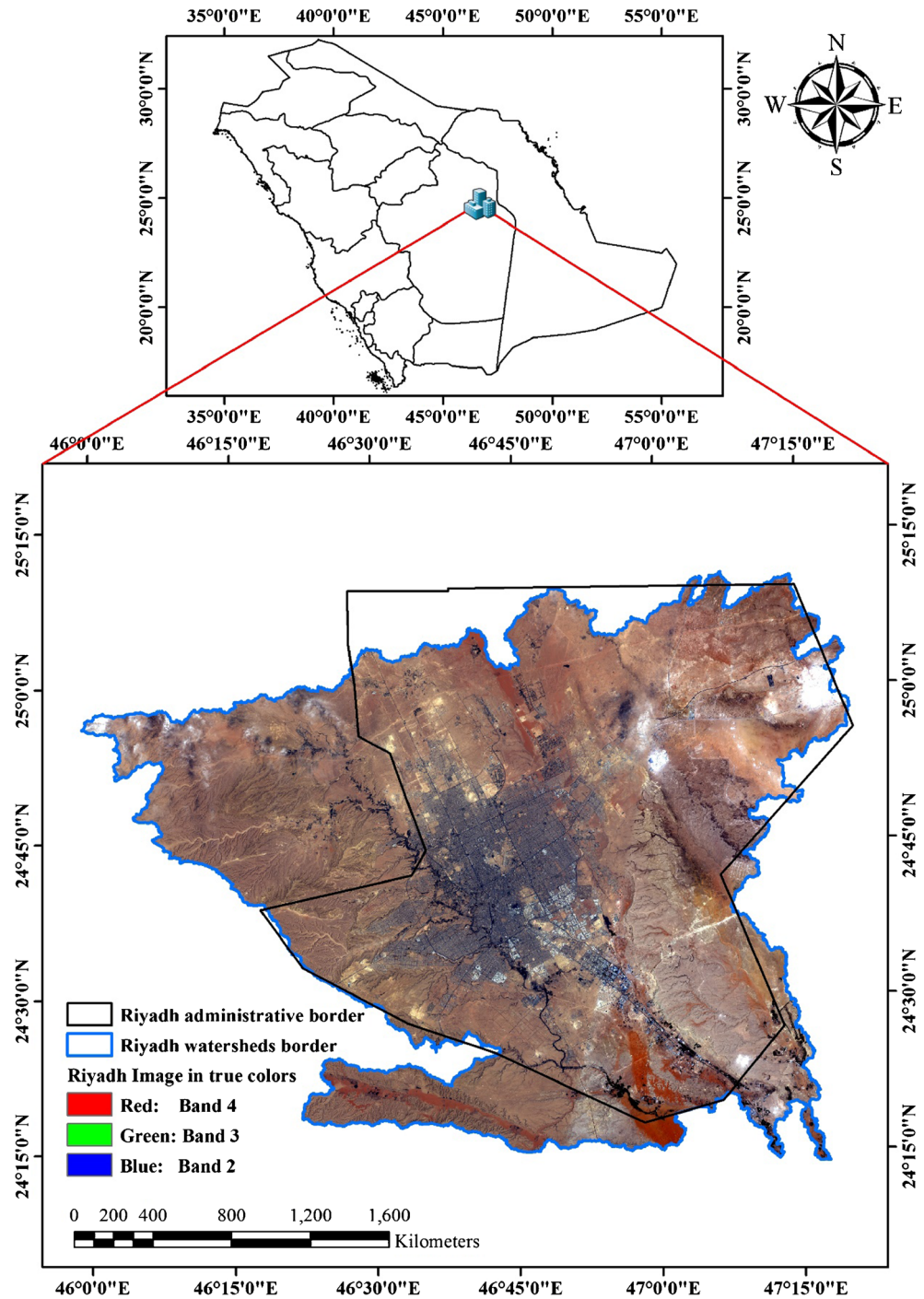
the inundation of cities, destruction of infrastructure, and loss of lives (Khan 2011; Mahmood and Mayo 2016; Mahmood and Ullah 2016; Ranjan 2017).

Therefore, this study aims to estimate the CN and potential direct runoff volume for urban watersheds of the Riyadh metropolitan area based on integrated GIS and RST data. Moreover, it provides a good regional case study for future assistance to the decision-makers in mitigating the flood risk, rainwater harvesting, and rainfall-runoff assessment.

Site descriptions

The study area is the urban city of Riyadh in the Kingdom of Saudi Arabia (KSA), located between latitude 24°13′51″ N to 25°10′30″ N and longitude 45°59′12″ E to 47°20′29″ E (Fig. 1). The area of the city is 6570 km^2 (including 1800 km^2 of urbanized area), while the watershed area measures about 8500 km^2. This urban area is characterized by horizontal expansion with vast infrastructure and agricultural and industrial areas

Fig. 1 Location map of Riyadh metropolitan area

Riyadh administrative border
Riyadh watersheds border
Riyadh Image in true colors
Red: Band 4
Green: Band 3
Blue: Band 2

0 200 400 800 1,200 1,600
Kilometers

(Rahman et al. 2016; Sharif et al. 2016). Additionally, demographically, Riyadh is one of the fastest growing cities with a high population intensity of 6.5 million people (Ashwan et al. 2012; Mahmoud and Gan 2019). The climate of Riyadh City is an extremely hot desert with sweltering temperatures during summer and a warm cool climate in winter. Despite a meager annual precipitation rate (Mahmoud and Gan 2018c) of about 62 mm, the city periodically experiences heavy rainfall events that lead to flash flooding.

Materials and methods

The potential runoff in the present is one of the most important factors of flood risk mitigation and rainfall water harvesting. It

Table 1   Data used in the study and sources (The year of use for all data is 2017)

Data	Data type	Data sources
DEM	1 Arc, 30 m	USGS
Soil map	JPEG image	MEWA
Geology map	JPEG image	SGS
Satellite image	Raster, 30 m	USGS
Precipitation	Records, daily	CFSR

USGS United States Geological Survey, *MEWA* Saudi Ministry of Environment, Water and Agriculture, *SGS* Saudi Geology Survey, *CFSR* Climate Forecast System Reanalysis

is estimated according to the NRCS-CN method. Mainly, this method is used to calculate the CN as a function of LULC and

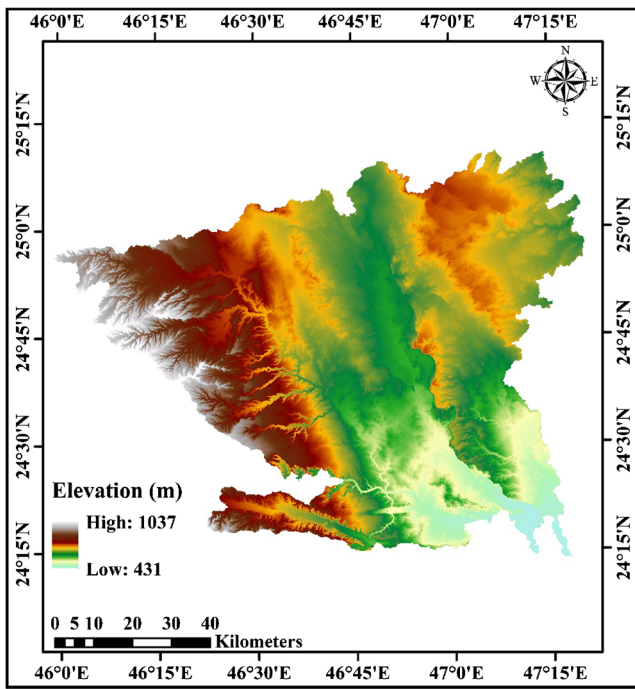**Fig. 2** Applied GIS-based methodology for the estimation curve number (CN) of the study area
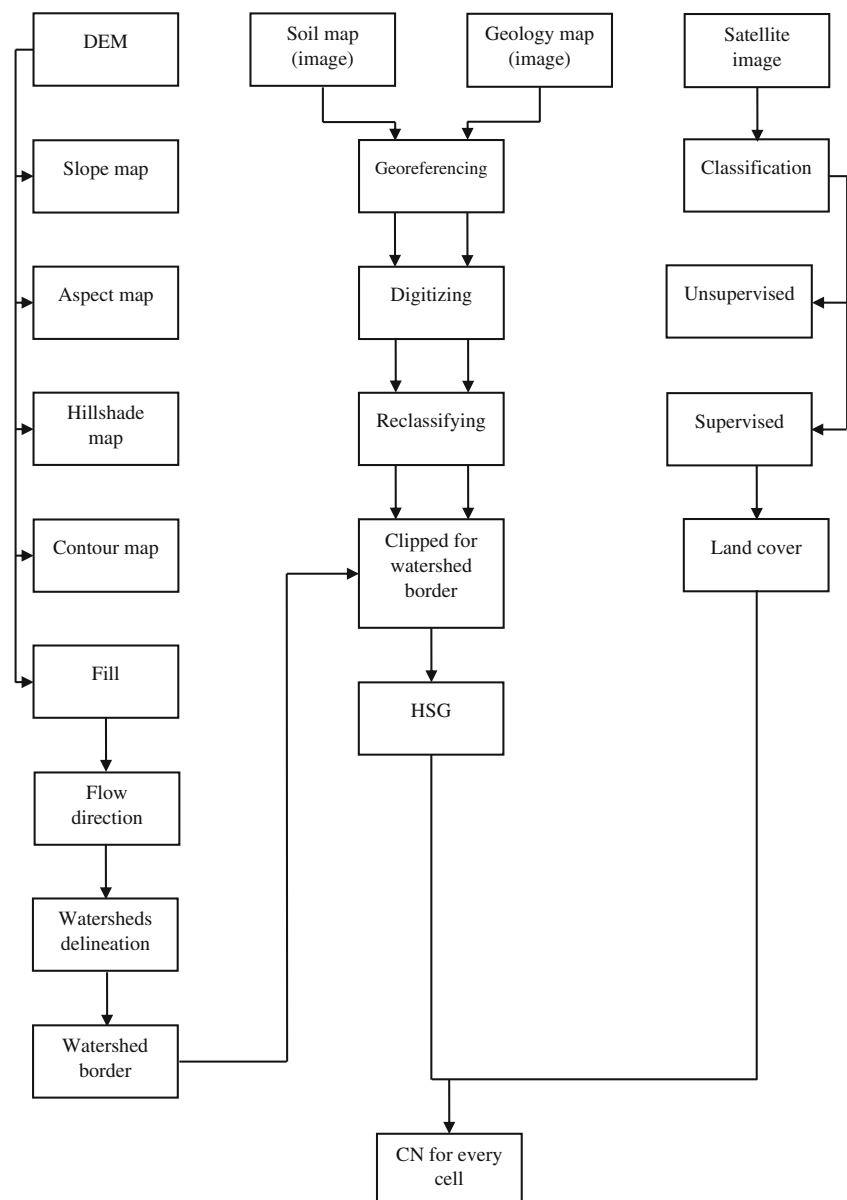
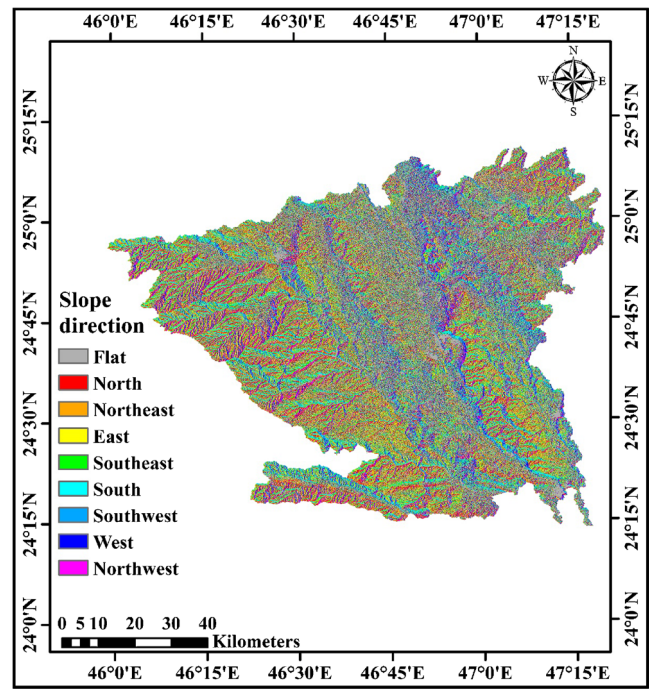**Fig. 3** Digital elevation model (DEM) of the study area

Fig. 5 Aspect map of the study area

HSG for the study area. Figure 2 illustrates the applied methodology for CN estimation and mapping, which employed DEM, soil map, geology map, and satellite image data as well as daily precipitation records (Table 1). The applied projection of this study is the WGS 84 UTM zone 38 coordinate system. Three steps have been used to calculate the CN based on available data as follows:

Firstly, DEM data of the United States Geological Survey (USGS) with a 30-m resolution (Fig. 3) was used to delineate the watersheds of the Riyadh metropolitan area with the aid of ArcGIS 10.4 platform. Besides, slope, aspect, hillshade, and contour maps were created, as shown in Figs. 4, 5, 6, and 7, respectively.

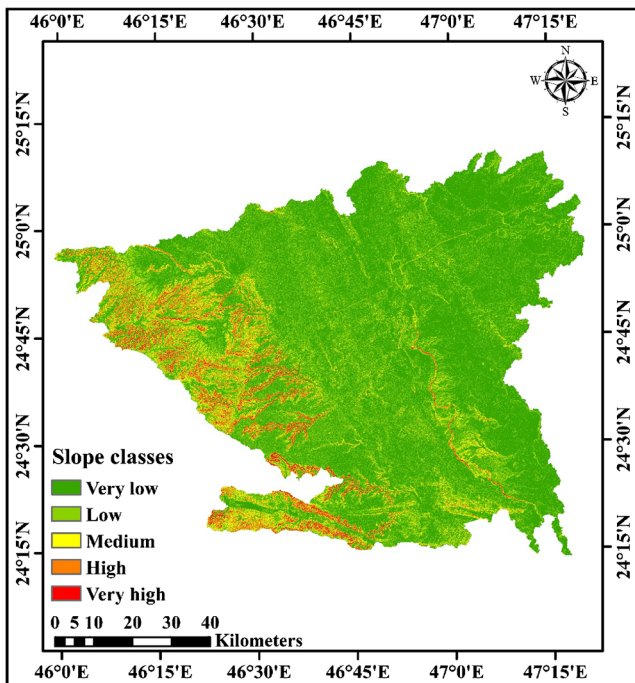Secondly, the HSG was developed for the study area by using a soil map (Fig. 8) and geologic map (Fig. 9) obtained

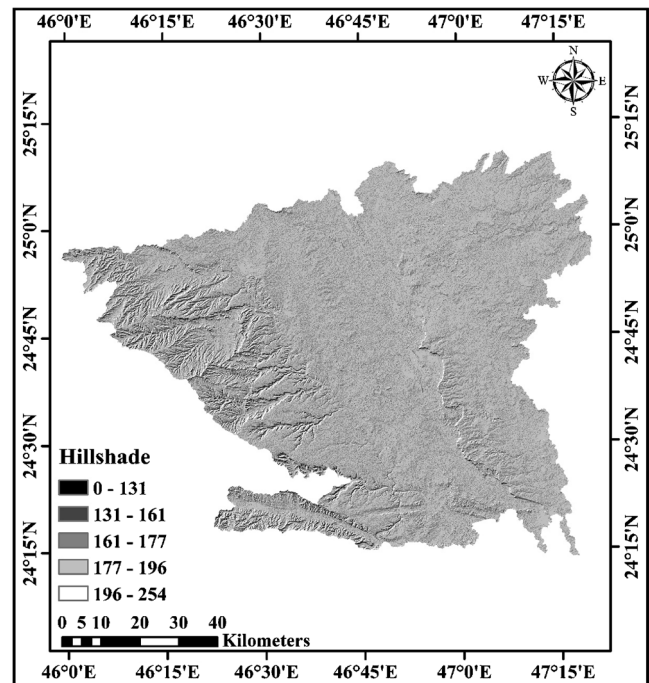

Fig. 4 Slope map of the study area
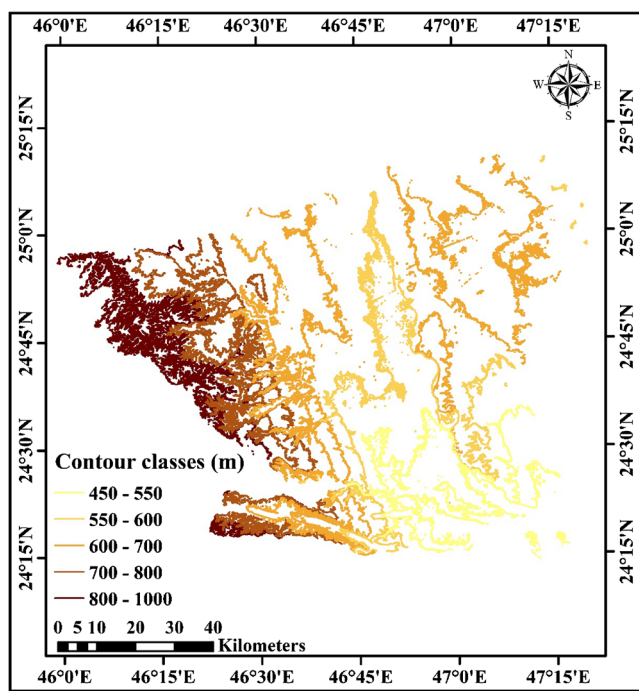

Fig. 6 Hillshade map of the study area
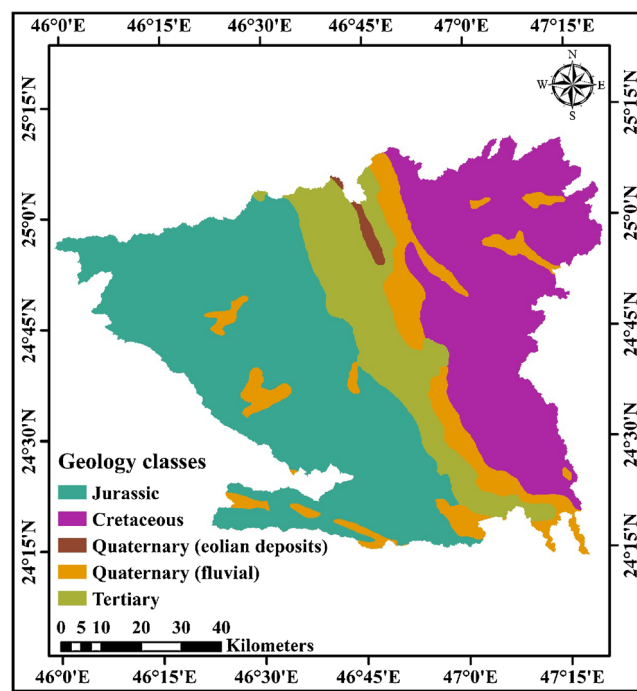
Fig. 7 Contour map of the study area

Fig. 9 Geology map of the study area

from the Saudi Ministry of Environment, Water and Agriculture (MEWA) and the Saudi Geology Survey (SGS), respectively. Both maps were downloaded as joint photographic experts group (JPEG) images, which require georeferencing, digitizing, reclassifying, and clipping. The soil map codes and their hydraulic conductivity data are listed in
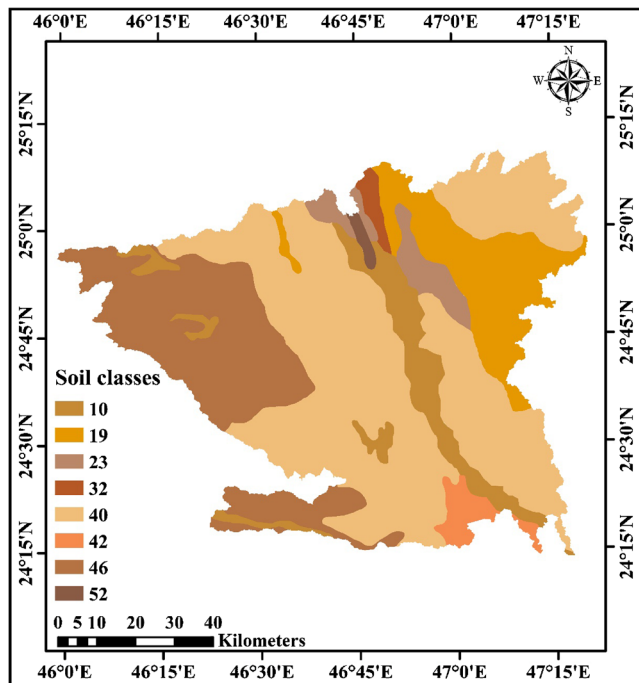
Table 2. The combination of these two maps resulted in the HSG classification.

Finally, the LULC was created for the study area by using a Landsat 8 image with 30 m resolution (Fig. 1). This image was retrieved from USGS and manipulated as unsupervised and supervised classifications by employing ENVI 5.3 software. The supervised map of the study area was classified into four land features: urban, barren land, agricultural land, and roads. The supervised classification of LULC is adopted for this study because it is more distinguishable than the unsupervised classification.

Estimation of the CN for every cell of the study area was performed using the combination tool incorporated in ArcGIS 10.4. Accordingly, the CN map was generated by combining

Fig. 8 Soil map of the study area

Table 2 Soil map codes with corresponding hydraulic conductivity (cm/h), water impermeable layer (cm), and soil texture at a water table depth of more than 150 cm (data available at http://gis.moa.gov.sa/gp/en/Default.aspx)

Soil code	Saturated hydraulic conductivity of the least transmissivity layer (cm/h)	Depth to water impermeable layer (cm)	Soil texture
10	1.5–5.1	> 150	Loam
23	1.5–5.1	25–50	Clay loam
32	1.5–5.1	25–100	Sandy clay loam
40	1.5–5.1	< 50	Clay loam
42	> 15	25–100	Sand
52	> 15	> 150	Sand

HSG and LULC maps under ARC II conditions (Table 3). The weighted area method was adopted to determine the weighted CN of each watershed in the study area, which was achieved by multiplying the value of the watershed CN by its area. Therefore, the following equations were used in developing the weighted CN map for each watershed.

$$Q = \frac{(P-I_a)^2}{(P-I_a) + S} \quad (1)$$

$$I_a = 0.05S \quad (2)$$

$$S = \frac{25400}{CN} - 254 \quad (3)$$

$$CN_w = \frac{\sum A_i CN_i}{\sum A_i} \quad (4)$$

Where CN_w is the weighted CN used for runoff volume computations; CN_i the CN of sub-area i; and A_i the area of sub-area i.

The CN values were adjusted for dry (I) and wet (III) ARC cases to avoid the unexpected jumps during the runoff estimation. Mishra et al. (2008) reported that the Sobhani formula (Sobhani 1976) and Hawkins formula (Hawkins et al. 1985) are the best conversion method for CN_I (Eq. 5) and CN_{III} (Eq. 6), respectively.

$$CN_I = \frac{CN_{II}}{2.334 - 0.01334CN_{II}} \quad (5)$$

$$CN_{III} = \frac{CN_{II}}{0.427 + 0.00573CN_{II}} \quad (6)$$

The potential runoff (Q) for every cell was then estimated by (1) determining the potential maximum retention after runoff begins (S) based on the CN value for each pixel, (2) calculating the initial abstraction (I_a), and (3) estimating the potential direct runoff according to the maximum daily rainfall data of CFSR (Fig. 10).

Table 3 Curve number (CN) values for land use/land cover (LULC) and hydrologic soil group (HSG) under all antecedent runoff conditions (ARC): I, II, III conditions

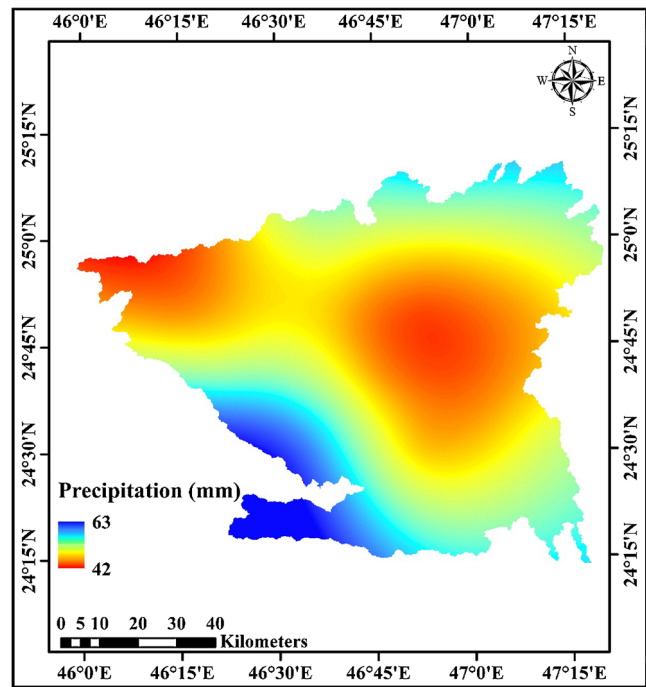| Land use/cover	Hydrologic soil group											
	A			B			C			D		
	I	II	III	I	II	III	I	II	III	I	II	III
Urban	78	89	95	83	92	96	87	94	97	89	95	98
Barren land	59	77	89	72	86	94	81	91	96	87	94	97
Agricultural land	43	64	81	55	74	87	65	81	91	71	85	93
Road	95	98	99	95	98	99	95	98	99	95	98	99

Fig. 10 Maximum daily precipitation distribution map of the study area

Results and discussion

The NRCS-CN method is widely used because of its ease of application and adaptability to small territories. According to the DEM, 40 watersheds with a total area of 8500 km^2 were delineated in the Riyadh metropolitan area as shown in Fig. 11. Table 4 describes each watershed and its characteristic
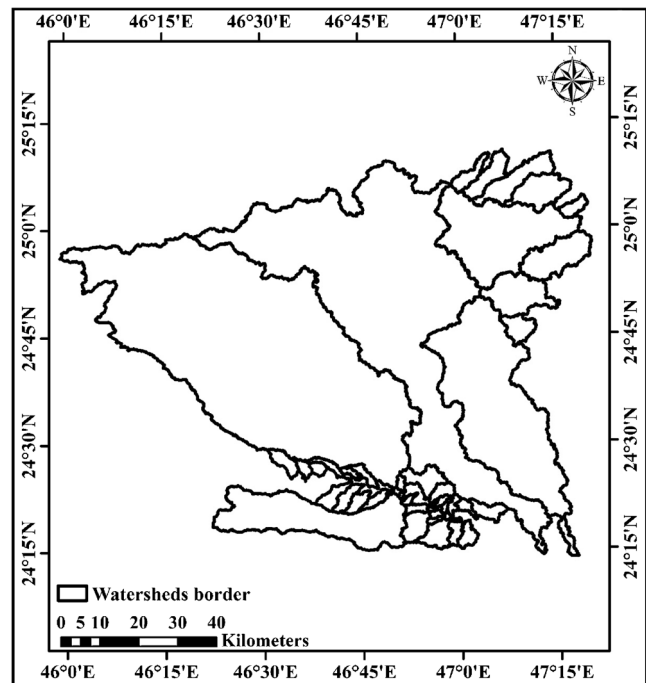

Fig. 11 Delineated watersheds of the study area

Table 4 Curve number (CN) of watersheds with hydrologic soil group (HSG)

HSG	Watershed no.	Area (km^2)	Average slope (%)	Watershed CN	Precipitation (mm)	S (mm)	I$_a$ (mm)	Q (mm)
A	1	22	6.8	77	58.2	75.87	3.79	22.72
	2	18	5.8	77	58.2	75.87	3.79	22.72
	3	12	9.9	77	52.7	75.87	3.79	19.17
	4	30	7.1	78	51.6	71.64	3.58	19.27
	5	10	8.2	80	50.9	63.50	3.18	20.48
B	6	141	2.9	86	45.7	41.35	2.07	22.40
	7	44	3.6	86	45.7	41.35	2.07	22.40
	8	132	2.8	88	45.7	34.64	1.73	24.59
C	9	515	2.8	90	47.9	28.22	1.41	28.93
D	10	45	4.6	91	58.2	25.12	1.26	39.51
	11	20	5.5	91	45.6	25.12	1.26	28.31
	12	2389	3.8	91	47.7	25.12	1.26	30.14
	13	6	5.9	91	50.9	25.12	1.26	32.96
	14	1013	3.4	92	47.6	22.09	1.10	31.52
	15	447	12.9	93	53.8	19.12	0.96	38.80
	16	6	4.9	93	45.6	19.12	0.96	31.26
	17	2945	8.8	94	47.8	16.21	0.81	34.94
	18	98	2.7	94	53.0	16.21	0.81	39.82
	19	33	2.5	94	53.0	16.21	0.81	39.82
	20	97	3.0	94	53.0	16.21	0.81	39.82
	21	22	2.6	94	53.0	16.21	0.81	39.82
	22	58	2.8	94	53.0	16.21	0.81	39.82
	23	49	3.6	94	45.6	16.21	0.81	32.89
	24	46	5.3	94	58.2	16.21	0.81	44.75
	25	28	13.2	94	52.0	16.21	0.81	38.88
	26	21	5.7	94	53.2	16.21	0.81	40.01
	27	16	6.2	94	45.6	16.21	0.81	32.89
	28	16	4.8	94	50.9	16.21	0.81	37.84
	29	12	6.4	94	58.2	16.21	0.81	44.75
	30	24	9.3	94	52.0	16.21	0.81	38.88
	31	12	17.3	94	56.0	16.21	0.81	42.66
	32	14	9.3	94	56.0	16.21	0.81	42.66
	33	27	16.5	94	56.0	16.21	0.81	42.66
	34	13	16.2	94	56.0	16.21	0.81	42.66
	35	3	11.4	94	56.0	16.21	0.81	42.66
	36	7	5.0	94	51.0	16.21	0.81	37.94
	37	1	7.9	94	45.6	16.21	0.81	32.89
	38	2	6.9	94	45.6	16.21	0.81	32.89
	39	7	4.2	94	45.6	16.21	0.81	32.89
	40	6	4.5	94	45.6	16.21	0.81	32.89

factors, as well as its corresponding CN and Q in millimeters. Watersheds 9, 12, 14, and 17 encompass more than 80% of the entire study area. Regarding the average slope of the watershed, only three watersheds, namely 31, 33, and 34, have an average terrain slope of more than 15% with an average maximum slope of 17.3, 16.5, and 16.2%, respectively. In addition, 35 watersheds have slopes less than 10%. Among these

watersheds, the lowest slope of which are 18, 19, and 21 by an average slope of 2.7, 2.5, and 2.6%, respectively.

Figure 12 depicts the HSG of the study area, which is characterized by four groups: A, B, C, and D. The HSG of D (clay loam) is the common obvious group, comprising about 71% of the total study area. This means that most of the area has high potential runoff and low infiltration rates
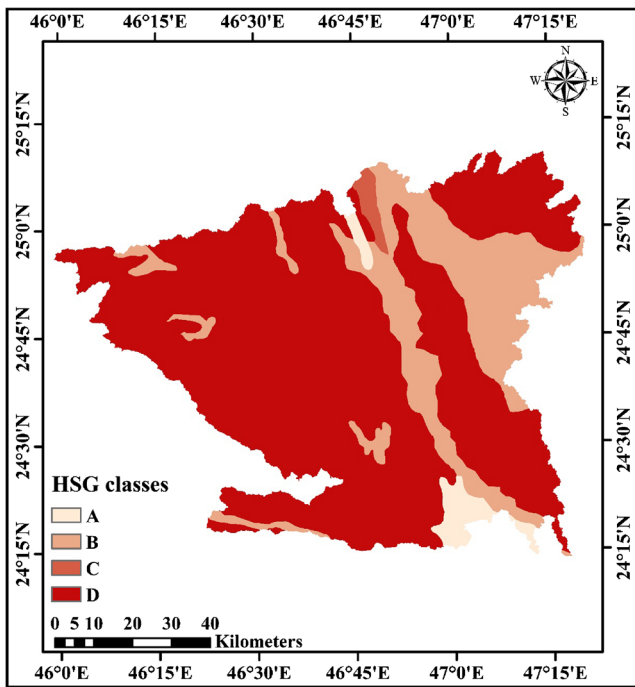
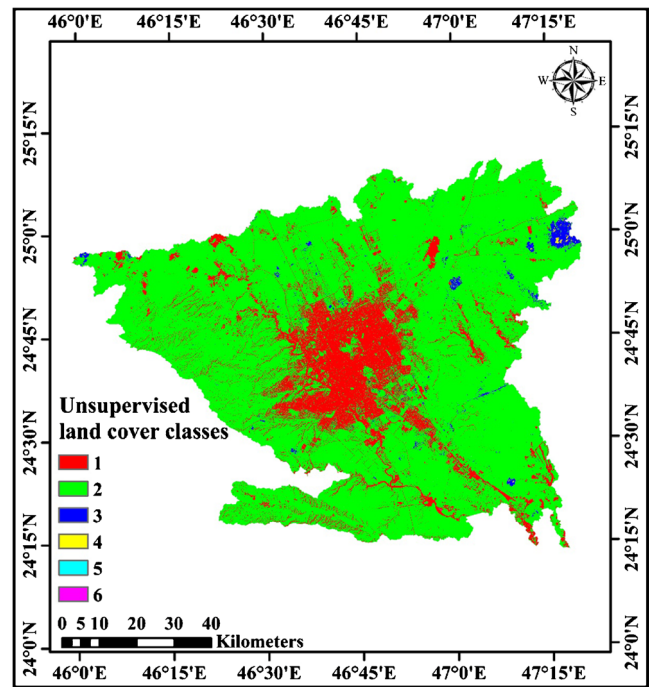Fig. 12 Hydrologic soil group (HSG) map of the study area

Fig. 13 Unsupervised land cover map of the study area

whereby water is transmitted finitely through the soil. These conditions indicate the presence of impervious materials therein. Group B (loam) follows in terms of coverage (26%). Whereas, groups A (sand) and C (sandy clay loam) do not exceed 5%. Therefore, the area is at risk of experiencing run-off during storm events.

Land cover is recognized as an essential parameter, affecting Q and flood behavior. In this study, both unsupervised and supervised classifications were used. Figure 13 shows the unsupervised land cover classes. Although this map has six classes (1 to 6), some land features such as the road layer do not appear. Thus, an unsupervised classification cannot adequately distinguish land cover types. Conversely, the supervised map can differentiate more details in the land cover. Figure 14 shows the supervised land cover of the study area, which consists of four land cover classes, namely urban, barren land, agricultural land, and roads. The majority of the study area is barren land, which covers 87.85% of the total area, while the land cover of urban areas, agricultural lands, and roads are 9, 1.5, and 1.65%, respectively. Moreover, barren land is on the outskirts of the study area, whereas the remaining land cover classes are concentrated in the center.

The CN values distributed in the study area for every cell from 64 to 98 are shown in Fig. 15. These CN values were used to calculate the weighted CN for every watershed (Fig. 16). Figures 15 and 16 confirm that about 80% of the watersheds have CN values higher than 90. The highest CN values cover barren, urban land, and roads, while the moderate CN values cover the agricultural land. These results indicate that the underlying lithology in the study area has high

impermeability in most places and a low amount of vegetation cover, leading to a high runoff and a very low infiltration rate. Therefore, the weighted CN of the study area is 92, which also emphasizes the previous result. The slope map illustrates that the slope is classified into five classes: very low (< 2.5), low (2.5–6.5), medium (> 6.5–12.5), high (> 12.5–20.5), and very high (> 20.5) degrees, where the slope varies from 0° to 52°. Hence, the study area slopes south to southeast, which is
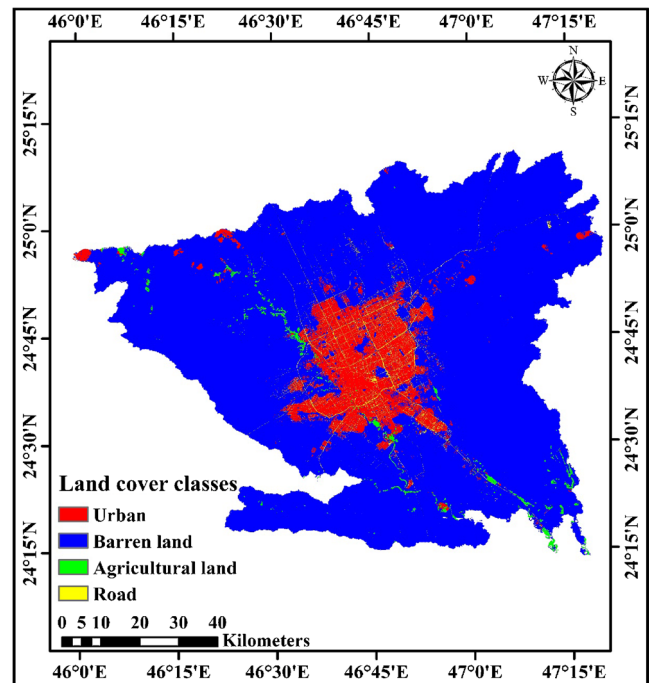

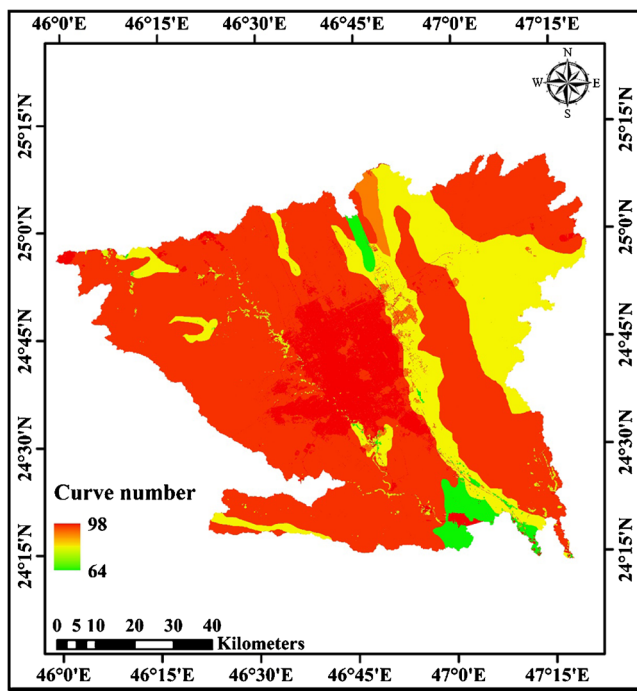Fig. 14 Supervised land cover map of the study area

Fig. 15 Curve number (CN) map for every cell of the study area

clearly indicated in the slope direction and hillshade maps. This evidence confirms the aforementioned nature of runoff and infiltration.

The maximum daily precipitation ranges from 42 to 63 mm from center to southwest of the city. Figure 17 classifies the potential maximum retention (S) into five classes: very low (< 19), low (19–31), medium (> 31–41), high (> 41–61), and very high (> 61) mm. Noteworthy is that the very low class
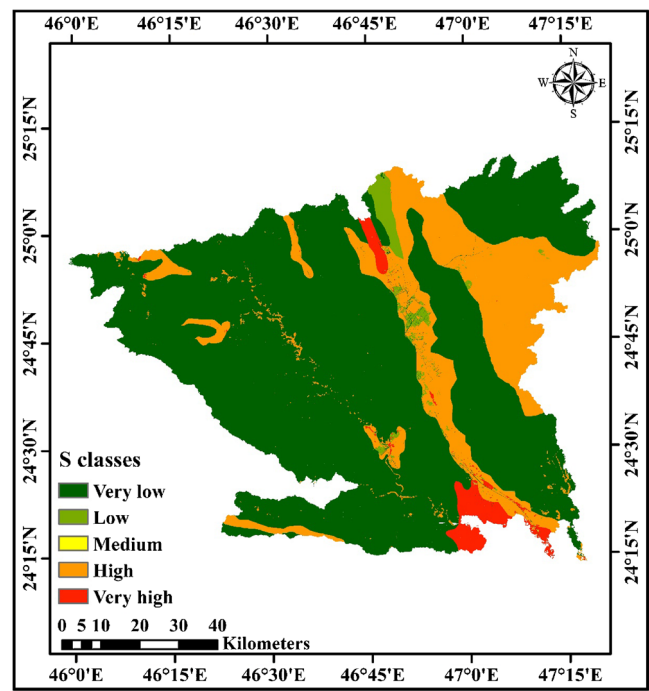
covers most of the study area and is widespread in the west and northwest, because the highest daily potential runoff depth is located in the same regions of the study area (Fig. 18). The runoff depth is also classified into five classes: very low (< 15), low (15–25), medium (> 25–35), high (> 35–50), and very high (> 50) mm. Therefore, monthly and annual runoff can be derived from the maximum daily runoff. The very low and low potential runoffs are restricted in the study

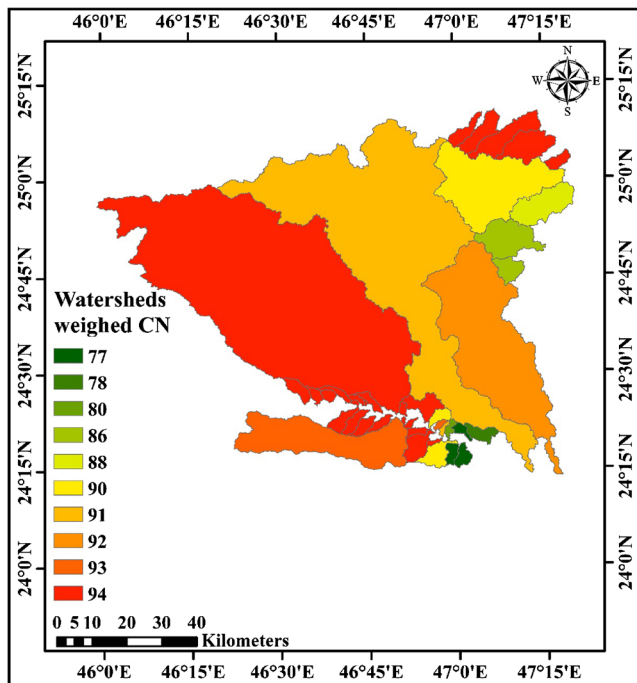Fig. 17 Potential maximum retention (S) map of the study area

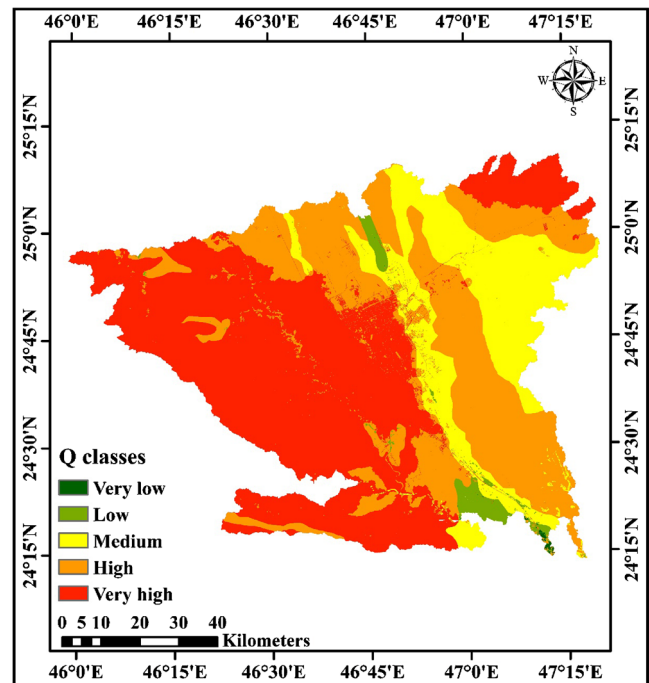Fig. 16 Weighed curve number (CN) map of the study area watersheds

Fig. 18 Potential runoff (Q) map of the study area

area, whereas the medium potential runoff has a low to moderate influence. High and very high runoffs threaten most places in the Riyadh metropolitan area, which can lead to catastrophic damages to property and harm to lives.

Conclusions

Flash flooding, a rapid and extreme effect of rainfall, is considered the worst flood type, because of the unexpected and devastating results thereof. Therefore, identifying the areas that may be at risk of flash flooding is crucial to help mitigate efforts. Hence, the NRCS-CN method and GIS were integrated to estimate the potential runoff for the Riyadh metropolitan area to augment output accuracy. The results show that the values of CN, precipitation, and runoff depth are 64–98, 42–63, and 10 to 59 mm, respectively.

Furthermore, 133 districts in the study area were shown to have very high potential runoff while only 8 districts demonstrated high potential runoff. This work was based on the integration of GIS and RST. The results can be used as an effective tool to help decision-makers in planning and managing watersheds for conducting more related studies in the area.

References

Abbas A, Amjath-Babu T, Kächele H, Müller K (2016) Participatory adaptation to climate extremes: an assessment of households' willingness to contribute labor for flood risk mitigation in Pakistan. J Water Clim Chang 7:621–636

Abdullah M, Feagin R, Musawi L (2017) The use of spatial empirical models to estimate soil erosion in arid ecosystems. Environ Monit Assess 189:1–17

Ahmad I, Verma V, Verma MK (2015) Application of curve number method for estimation of runoff potential in GIS environment. Paper presented at the 2nd International Conference on Geological and Civil Engineering

Ajmal M, Kim T-W (2014) Quantifying excess stormwater using SCS-CN-based rainfall runoff models and different curve number determination methods. J Irrig Drain Eng 141:1–12

Ajmal M, Waseem M, Ahn J-H, Kim T-W (2016) Runoff estimation using the NRCS slope-adjusted curve number in mountainous watersheds. J Irrig Drain Eng 142:1–12

Anaba LA, Banadda N, Kiggundu N, Wanyama J, Engel B, Moriasi D (2017) Application of SWAT to assess the effects of land use change in the Murchison Bay catchment in Uganda. Comput Water Energy Environ Eng 6:24–40

Angelakis A (2016) Evolution of rainwater harvesting and use in Crete, Hellas, through the millennia. Water Sci Technol Water Supply 16: 1624–1638

Archer D, Fowler H (2015) Characterising flash flood response to intense rainfall and impacts using historical information and gauged data in Britain. J Flood Risk Manag 11:S121–S133

Ashwan MSA, Salam AA, Mouselhy MA (2012) Population growth, structure and distribution in Saudi Arabia. Humanit Soc Sci Rev 1:33–46

Beck HE, de Jeu RA, Schellekens J, van Dijk AI, Bruijnzeel LA (2009) Improving curve number based storm runoff estimates using soil moisture proxies. IEEE J Sel Top Appl Earth Obs Remote Sens 2: 250–259

Bhagat N (2016) Estimation of SCS-CN for lower Mahi basin, Gujarat, India. Int J Adv Eng Res Technol 4:61–63

Chavda DB, Makwana JJ, Parmar HV, Kunapara AN, Prajapati GV (2016) Estimation of runoff for Ozat catchment using RS and GIS based SCS-CN method. Curr World Environ 11:212–217

Cronshey R (1986) Urban hydrology for small watersheds. US Dept. of Agriculture, Soil Conservation Service, Engineering Division

Dale M, Clarke J, Harris H (2016) Urban flood prediction and warning—challenges and solutions. Proc Water Environ Fed 2016:2237–2242

Deng L, McCabe MF, Stenchikov G, Evans JP, Kucera PA (2015) Simulation of flash-flood-producing storm events in Saudi Arabia using the weather research and forecasting model. J Hydrometeorol 16:615–630

Dile YT, Srinivasan R (2014) Evaluation of CFSR climate data for hydrologic prediction in data-scarce watersheds: an application in the Blue Nile River basin. JAWRA J Am Water Resour Assoc 50:1226–1241

Durán-Barroso P, González J, Valdés JB (2016) Improvement of the integration of soil moisture accounting into the NRCS-CN model. J Hydrol 542:809–819

Ebrahimian M (2012) Application of NRCS-curve number method for runoff estimation in a mountainous watershed. Caspian J Environ Sci 10:103–114

Ebrahimian M, See LF, Ismail MH, Malek IA (2009) Application of natural resources conservation service–curve number method for runoff estimation with GIS in the Kardeh watershed, Iran. Eur J Sci Res 34:575–590

Elfeki A, Masoud M, Niyazi B (2017) Integrated rainfall–runoff and flood inundation modeling for flash flood risk assessment under data scarcity in arid regions: Wadi Fatimah basin case study, Saudi Arabia. Nat Hazards 85:87–109

Fisher P, Comber AJ, Wadsworth R (2005) Land use and land cover: contradiction or complement. In: Fisher P (ed) Re-presenting GIS. Wiley, England, pp 85–98

Fuka DR, Walter MT, MacAlister C, Degaetano AT, Steenhuis TS, Easton ZM (2014) Using the Climate Forecast System Reanalysis as weather input data for watershed models. Hydrol Process 28:5613–5623

Gajbhiye S, Mishra S, Pandey A (2014) Relationship between SCS-CN and sediment yield. Appl Water Sci 4:363–370

GhaffarianHoseini A, Tookey J, GhaffarianHoseini A, Yusoff SM, Hassan NB (2016) State of the art of rainwater harvesting systems towards promoting green built environments: a review. Desalin Water Treat 57:95–104

Harish N, Hemalatha T, Babu CM (2016) Sensitivity of curve number and initial abstraction coefficient on SCS-CN method of runoff estimation in an ungauged watershed integrated with RS & GIS. PARIPEX-Indian J Res 4:50–52

Hawkins RH, Hjelmfelt AT Jr, Zevenbergen AW (1985) Runoff probability, storm depth, and curve numbers. J Irrig Drain Eng 111:330–340

Hoedjes JC, Kooiman A, Maathuis B, Said M, Becht R, Limo A, Mumo M, Nduhiu-Mathenge J, Shaka A, Su B (2014) A conceptual flash flood early warning system for Africa, based on terrestrial microwave links and flash flood guidance. ISPRS Int J Geo-Inf 3:584–598

Hong Y, Adler RF, Hossain F, Curtis S, Huffman GJ (2007) A first approach to global runoff simulation using satellite rainfall estimation. Water Resour Res 43:1–8

Jaber HS, Mansor S, Pradhan B, Ahmad N (2016) Rainfall–runoff modelling and water balance analysis for Al-Hindiyah barrage, Iraq using remote sensing and GIS. Geocarto Int 32:1407–1420

Karagiorgos K, Thaler T, Hübl J, Maris F, Fuchs S (2016) Multi-vulnerability analysis for flash flood risk management. Nat Hazards 82:63–87

Khan AN (2011) Analysis of flood causes and associated socio-economic damages in the Hindukush region. Nat Hazards 59:1239–1260

Lal M et al (2016) Evaluation of the Soil Conservation Service curve number methodology using data from agricultural plots. Hydrogeol J 25:151–167

Lee RS, Traver RG, Welker AL (2016) Evaluation of soil class proxies for hydrologic performance of in situ bioinfiltration systems. J Sustain Water Built Environ 2:1–10

Li R, Rui X, Zhu A-X, Liu J, Band LE, Song X (2015) Increasing detail of distributed runoff modeling using fuzzy logic in curve number. Environ Earth Sci 73:3197–3205

Mack B, Leinenkugel P, Kuenzer C, Dech S (2017) A semi-automated approach for the generation of a new land use and land cover product for Germany based on Landsat time-series and Lucas in-situ data. Remote Sens Lett 8:244–253

Mahmood S, Mayo SM (2016) Exploring underlying causes and assessing damages of 2010 flash flood in the upper zone of Panjkora River. Nat Hazards 83:1213–1227

Mahmood S, Ullah S (2016) Assessment of 2010 flash flood causes and associated damages in Dir Valley, Khyber Pakhtunkhwa Pakistan. Int J Disaster Risk Reduct 16:215–223

Mahmoud SH, Gan TY (2018a) Impact of anthropogenic climate change and human activities on environment and ecosystem services in arid regions. Sci Total Environ 633:1329–1344

Mahmoud SH, Gan TY (2018b) Long-term impact of rapid urbanization on urban climate and human thermal comfort in hot-arid environment. Build Environ 142:83–100

Mahmoud SH, Gan TY (2018c) Multi-criteria approach to develop flood susceptibility maps in arid regions of Middle East. J Clean Prod 196:216–229

Mahmoud SH, Gan TY (2018d) Urbanization and climate change implications in flood risk management: developing an efficient decision support system for flood susceptibility mapping. Sci Total Environ 636:152–167

Mahmoud SH, Gan TY (2019) Irrigation water management in arid regions of Middle East: assessing spatio-temporal variation of actual evapotranspiration through remote sensing techniques and meteorological data. Agric Water Manag 212:35–47

Masseroni D, Cislaghi A, Camici S, Massari C, Brocca L (2016) A reliable rainfall–runoff model for flood forecasting: review and application to a semi-urbanized watershed at high flood risk in Italy. Hydrol Res 48:726–740

Mishra SK, Singh V (2013) SCS-CN method. In: Soil conservation service curve number (SCS-CN) methodology, vol 42. Springer, Dordrecht, pp 84–146

Mishra S, Jain M, Babu PS, Venugopal K, Kaliappan S (2008) Comparison of AMC-dependent CN-conversion formulae. Water Resour Manag 22:1409–1420

Mistry A, Lodha P, Prakash I, Mehmood K (2017) Estimation of direct runoff for purna river sub-basin, using SCS-CN method, Dangs District, Gujarat. Int J Adv Eng Res Dev 4:581–593

Moon G-W, Ajmal M, Ahn J-H, Kim T-W (2016) Investigating practical alternatives to the NRCS-CN method for direct runoff estimation using slope-adjusted curve numbers. KSCE J Civ Eng 20:3022–3030

Nonglait TL, Tiwari B (2016) Application of SCS-CN method for estimation of runoff in a humid microwatershed. Int J Curr Agric Sci 6:121–127

NRCS (2007) National Engineering Handbook: part 630—hydrology. USDA Soil Conservation Service, Washington, DC, USA. Available online at https://directives.sc.egov.usda.gov/viewerFS.aspx?hid=21422

NRCS (2009) National engineering handbook: part 630—hydrology. USDA Soil Conservation Service, Washington, DC, USA.

Available online at https://directives.sc.egov.usda.gov/viewerFS.aspx?hid=21422

Oliveira P, Nearing M, Hawkins R, Stone J, Rodrigues D, Panachuki E, Wendland E (2016) Curve number estimation from Brazilian Cerrado rainfall and runoff data. J Soil Water Conserv 71:420–429

Patel GR, Trivedi MM (2016) Prediction and validation of runoff through RS and GIS-based distributed SCS-CN method. Adv Life Sci 5:4965–4977

Patil J, Sarangi A, Singh A, Ahmad T (2008) Evaluation of modified CN methods for watershed runoff estimation using a GIS-based interface. Biosyst Eng 100:137–146

Pitt R (1999) Small storm hydrology and why it is important for the design of stormwater control practices. J Water Manag Model 7:61–91

Rahman MT, Aldosary AS, Nahiduzzaman KM, Reza I (2016) Vulnerability of flash flooding in Riyadh, Saudi Arabia. Nat Hazards 84:1807–1830

Rajeevan M (2017) Past and future trends of hydroclimatic intensity over the Indian monsoon region. J Geophys Res Atmos 122:896–909

Ranjan R (2017) Flood disaster management. In: Sharma N (ed) River system analysis and management. Springer, Singapore, pp 371–417

Ryu J, Jung Y, Kong DS, Park BK, Kim YS, Engel BA, Lim KJ (2016) Approach of land cover based asymptotic curve number regression equation to estimate runoff. Irrig Drain 65:94–104

Salih AA, Hamid AA (2017) Hydrological studies in the White Nile State in Sudan. Egypt J Remote Sens Space Sci 20:S31–S38

Sartori A, Hawkins RH, Genovez AM (2011) Reference curve numbers and behavior for sugarcane on highly weathered tropical soils. J Irrig Drain Eng 137:705–711

Shadeed S, Almasri M (2010) Application of GIS-based SCS-CN method in West Bank catchments, Palestine. Water Sci Eng 3:1–13

Shah M, Bhagat N (2017) Estimation of weighted SCS-CN: case of Narmada river basin, India. Int J Sci Res 5:687–688

Sharif HO, Al-Juaidi FH, Al-Othman A, Al-Dousary I, Fadda E, Jamal-Uddeen S, Elhassan A (2016) Flood hazards in an urbanizing watershed in Riyadh, Saudi Arabia. Geomat Nat Haz Risk 7:702–720. https://doi.org/10.1080/19475705.2014.945101

Shi Z-H, Chen L-D, Fang N-F, Qin D-F, Cai C-F (2009) Research on the SCS-CN initial abstraction ratio using rainfall-runoff event analysis in the Three Gorges Area, China. Catena 77:1–7

Singh LK, Jha MK, Chowdary V (2017) Multi-criteria analysis and GIS modeling for identifying prospective water harvesting and artificial recharge sites for sustainable water supply. J Clean Prod 142:1436–1456

Sobhani G (1976) A review of selected small watershed design methods for possible adoption to Iranian conditions. M.S. Thesis, Utah State University, Logan, UT

Starosolszky O, Melder O (2014) Hydrology of disasters. Routledge, Geneva

Tirkey AS, Ghosh M, Pandey A, Shekhar S (2017) Assessment of climate extremes and its long term spatial variability over the Jharkhand State of India. Egypt J Remote Sens Space Sci 21:49–63

Wang F, Ge Q, Yu Q, Wang H, Xu X (2017) Impacts of land-use and land-cover changes on river runoff in Yellow River basin for period of 1956-2012. Chin Geogr Sci 27:13–24

Woodward DE, Hawkins RH, Jiang R, Hjelmfelt J, Allen T, Van Mullem JA, Quan QD (2003) Runoff curve number method: examination of the initial abstraction ratio. In: World Water & Environmental Resources Congress 2003, pp 1–10

Yuan Y, Nie W, McCutcheon SC, Taguas EV (2014) Initial abstraction and curve numbers for semiarid watersheds in Southeastern Arizona. Hydrol Process 28:774–783

Zhang Q, Luo G, Li L, Zhang M, Lv N, Wang X (2017) An analysis of oasis evolution based on land use and land cover change: a case study in the Sangong River basin on the northern slope of the Tianshan Mountains. J Geogr Sci 27:223–239